NUMERICAL SIMULATION OF SINGLE-NOZZLE LARGE SCALE SPRAY COOLING ON DRUM WALL

by

Zuobing CHEN[a], Qiang XIE[a,*], Gong CHEN[b], Yongjie YU[a], and Zheyu ZHAO[a]

[a] School of Mechanical and Electronic Engineering, Wuhan University of Technology, Wuhan, Hubei, China
[b] Sinoma (Suzhou) Construction, Ltd., Kunshan, Jiangsu, China

Original scientific paper
https://doi.org/10.2298/TSCI170920243C

In this work the single-nozzle spray cooling on a large scale industry-used drum wall has been simulated by a verified numerical model. For a certain spray nozzle, the effects of four parameters, i. e. different spray pressures, different spray heights, different water temperatures, and different wall temperatures, on heat transfer have been analyzed. It is found that the mean heat flux distributions show concentric elliptical circles. Increasing spray pressures will enhance the cooling performance. Decreasing spray heights will improve the heat flux in direct spray areas other than whole simulated drum wall. As expected, reducing water temperature or advancing wall temperature will raise the average wall flux. Both relationships are exponential. The influencing degrees of the four parameters have been compared through Taguchi orthogonal experimental method and the result is: wall temperature > spray pressure > water temperature > spray height. The wall temperature, spray pressure, and water temperature show dominant effects except for the spray height.

Key words: *numerical simulation, drum wall, single-nozzle, spray cooling, large scale*

Introduction

Spray cooling happens when liquid is atomized by specific devices such as nozzles into fine droplets which then impact on a heated surface. These droplets can spread on the surface, form a liquid film and/or evaporate directly or indirectly, removing large quantity of heat due to the latent heat of evaporation as well as substantial convection [1]. As a consequence it has been widely used in numerous applications such as electronic chip cooling [2], skin protection during medical treatment [3], alloy quenching in metallurgy [4], and superheated steam cooling [5].

Considerable studies have been conducted to understand spray cooling due to its high-flux removal ability and complexity. Firstly on heat transfer mechanisms, for example Liang, and Mudawar [6, 7] concluded that according to liquid boiling curves the spray cooling have different regimes including single-phase liquid cooling and nucleate boiling regimes with relatively high flux, low temperature mechanisms, and relatively high temperature transition boiling and film boiling regimes. Secondly on heat transfer enhancement, one way to im-

* Corresponding author, e-mail: johnarmstrong@whut.edu.cn; qiangxie_whut@163.com

prove the heat removal ability is to change the cooling medium characteristics such as using nanofluids instead of pure liquids [8, 9] and adding surfactants with a suitable concentration [10]. Another one is to change the structures of the flat heated surface such as increasing surface roughness [11] and processing fins [12, 13] and other micro-structures [14]. Thirdly on flow characteristics this aspect includes several fields such as droplet dynamics [15], discharging rates [16], and flow structures. For example, Vouros, *et al.* [17] studied experimentally the influence of heated surface on the development of jet sprays and found that heat flux from heated surface would influence the evolution of spray jet.

The previous studies have made some achievements and promoted the development of spray cooling technology as well as the understanding of spray cooling fundamentals especially thanks to advanced experimental devices like the phase Doppler anemometry. Nevertheless there are still many problems. For example, most research results come from small-scale laboratory experiments and the objects of study are always flat heated surfaces. The results can not be directly introduced into large-scale industrial applications without any similarity criterions. For example, fig. 1 shows a schematic of a patented product named as spray cooling rotary drum cooler. It is a downstream equipment of rotary hearth furnace for cooling direct-reduced iron (DRI) [18] from about 1400-500 K. Up to now it has already been used on many DRI production lines of steel-making industry in China. It always has several meters in diameter and tens of meters in length. The spray cooling system is so much different with those in laboratory-scale. For example the nozzles are always bigger which ensures high flow rate and low blocking possibility and the spray height is much greater for easy maintenance and less nozzle quantities. Even though the equipment has been in use, it is necessary to establish new understandings which will help the design, operation and optimization of the large-scale applications. Inspired by the considerations the numerical simulation method is employed to analyze the spray cooling performance under different conditions.

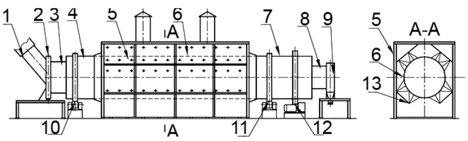

Figure 1. Structure schematic of a spray cooling rotary drum cooler for reduced iron; *1 – feeding chute, 2 – feeding cabin, 3 – feeding drum, 4 – front-end double-shell drum, 5 – shield, 6 – main drum, 7 – tail-end double-shell drum, 8 – discharging drum, 9 – discharging cabin, 10 – front-end supporting roller, 11 – tail-end supporting roller, 12 – drive system, 13 – spray system*

Model description

Physical model

The physical model comes from an industry-used spray cooling drum, see fig. 1. Only one nozzle spray on a local part of the steel drum wall is the object of study. The outer diameter of the wall with thickness about 40 mm is 3.08 m, the center angle of the focused part is 60 degree (corresponding arc length 1.6 m) and the width (length in drum axis direction) is 1.0 m, which ensures full development of the spray, fig. 2(a). The wall is considered to have uniform temperature and be stationary based on following reasons. Firstly the spray cooling heat flux is usually up to 10^6 W/m^2 while the wall has large thermal conductivity. Most importantly the wall has an extremely low rotating speed (usually 1-3 rpm) in real practice. The nozzle is solid-cone pressure swirl which is most commonly used due to its simple geometry and excellent atomizing performance [16].

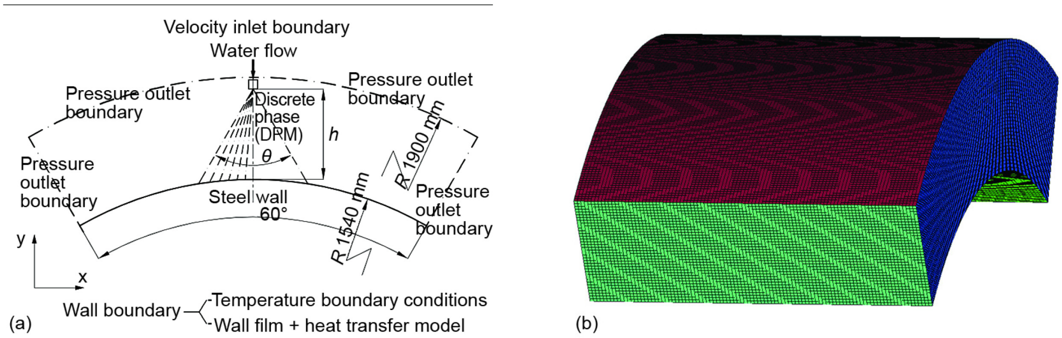

Figure 2. (a) The boundary conditions of simulated system (single nozzle at standard atmosphere), (b) the computational mesh

Numerical model

Continuous phase model

The continuous phase is treated as incompressible and ideal air flow which always follows three conservation laws, *i. e.* mass conservation, momentum conservation and energy conservation. As the theory details could be found in [19], the three laws are briefly introduced here and they are, respectively, given by:

$$\frac{\partial \rho}{\partial t} + \nabla(\rho \vec{\mathrm{U}}) = S_{\mathrm{m}} \tag{1}$$

$$\frac{\partial}{\partial t}(\rho \vec{\mathrm{U}}) + \nabla(\rho u \vec{\mathrm{U}}) = \nabla(\eta \nabla \vec{\mathrm{U}}) - \nabla p + S_{\mathrm{f}} \tag{2}$$

$$\frac{\partial}{\partial t}(\rho E) + \nabla[\vec{\mathrm{U}}(\rho E + p)] = \nabla\left(k_{\mathrm{eff}} \nabla T - \sum_j J_j \int_{T_{\mathrm{ref}}}^{T} c_{p,j} \mathrm{d}T + \tau_{\mathrm{eff}} \vec{\mathrm{U}}\right) + S_{\mathrm{h}} \tag{3}$$

where S_{m} is the added mass in the continuous phase. Three terms:

$$k_{\mathrm{eff}} \nabla T, \qquad \sum_j J_j \int_{T_{\mathrm{ref}}}^{T} c_{p,j} \mathrm{d}T, \qquad \text{and} \qquad \tau_{\mathrm{eff}} \vec{\mathrm{U}}$$

indicate heat energy transferred, respectively, by conduction, by component diffusion, and by viscous dissipation. The k_{eff} is the effective conductivity, T_{ref} – the reference temperature, S_{h} – the volume heat source terms caused by heat transfer between droplets and continuous phase.

Discrete phase model

Changes of motion and thermodynamics of the discrete phase (droplets) in the continuous phase (air) will happen due to interaction (contact or collision) with other droplets or boundaries. The droplet trajectory could be calculated by the differential equations of forces which in inertial co-ordinate systems given by:

$$\frac{\mathrm{d}u_{\mathrm{p}}}{\mathrm{d}t} = F_{\mathrm{D}}(u - u_{\mathrm{p}}) + \frac{\mathrm{g}(\rho_{\mathrm{p}} - \rho)}{\rho_{\mathrm{p}}} \tag{4}$$

where F_D is given by:

$$F_D = \frac{18\mu}{\rho_p d_p^2} \frac{C_D \,\mathrm{Re}}{24} \tag{5}$$

where C_D is the dynamic drag coefficient and it is calculated by:

$$C_D = \begin{cases} 0.424 & \mathrm{Re} > 1000 \\ \dfrac{24}{\mathrm{Re}}\left(1 + \dfrac{1}{6}\mathrm{Re}^{2/3}\right) & \mathrm{Re} \le 1000 \end{cases} \tag{6}$$

According to different thermal conditions, the droplets would follow three laws, *i. e.* evaporation, inert heating, and boiling. Phase change happens slowly during vaporization and fast during boiling. The droplet temperatures could be calculated by the heat balance equation which is expressed:

$$m_p c_p \frac{dT_p}{dt} = hA_p(T_f - T_p) - \frac{dm_p}{dt} h_{fg} + A_p \varepsilon_p \sigma(\theta_R^4 - T_p^4) \tag{7}$$

where h is the heat transfer coefficient which is given by:

$$\mathrm{Nu} = \frac{hd_p}{k_\infty} = 2.0 + 0.6\sqrt{\mathrm{Re}_d}\sqrt[3]{\mathrm{Pr}} \tag{8}$$

For interactions with wall, the wall-film model is applied which is a specific condition for simulation of liquid droplets colliding with walls and forming thin films. Four regimes, *i. e.* stick, rebound, spread, and splash are based on the impact energy and wall temperature [19]. The critical temperature factor is set to be 1.0 and Stanton-Rutland impinging and splashing model is applied.

Discrete phase and continuous phase coupling

After the discrete phase is added to the continuous phase, the two phases will interact with each other in terms of mass, momentum and energy. When the droplet particles pass through the fluid domain the mass change is given by:

$$M = \frac{\Delta m_p}{m_{p,0}} \dot{m}_{p,0} \tag{9}$$

The change in momentum is expressed:

$$F = \sum \left[\frac{18\beta\mu C_D \,\mathrm{Re}}{24\rho_p d_p^2} (u_p - u)\dot{m}_p \Delta t \right] \tag{10}$$

The energy change E is calculated by:

$$E = \frac{\dot{m}_{p,0}}{m_{p,0}} \left[\Delta m_p (h_{pyrol} - h_{fg}) + m_{p_{in}} \int_{T_{ref}}^{T_{p_{in}}} c_{p_p} dT - m_{p_{out}} \int_{T_{ref}}^{T_{p_{out}}} c_{p_p} dT \right] \tag{11}$$

Simulation procedure and conditions

Table 1. Simulation conditions

Parameter	Base value (variation range)
Wall temperature, [K]	673 (373-673)
Water temperature, [K]	282 (282-298)
Nozzle type and orifice diameter, [mm]	Solid-cone pressure swirl, 2.0
Spray angle, [°]	60
Spray height, [m]	0.36 (0.27-0.36)
Upstream spray pressure, [MPa]	0.6 (0.3-0.6)
Spray flow rate, [kgs^{-1}]	0.1 (0.0707-0.1)

The studies are carried out by following geometry building, mesh generation, boundary setting, mesh independence check, and formal simulations in sequence. In the simulations the Euler-Lagrangian method is employed to model the two phase flow based on ANSYS Fluent package Release 17.0. At the beginning the continuous phase flow field is calculated. And then droplets are injected and changes of trajectories, velocity and energy of the discrete phase are computed. Finally, the mass, momentum and energy change are taken as source terms into the continuous phase flow for coupling until convergence happens by monitoring the droplet flow and heat transfer processes. The simulation conditions are listed in tab. 1.

Model validation

The numerical model needs to be validated in order to obtain correct results. The spray cooling with same conditions as physical experiments [11] have been simulated on a small and flat heated surface. The nozzle has a spray half angle 30° and an orifice diameter 1.0 mm. The spray medium is deionized water with temperature 25 °C. The spray height is 15 mm and the effective flow rate is 41.6 L/h under an upstream pressure 0.3 MPa. The heated surface is copper with diameter 12 mm. Experiment details could be found in [11]. Computing domain geometry is built in size 25 × 25 × 25 mm (length×width×heigth) with symmetrical boundaries on both x- and y-directions, ensuring enough space for spray development. The local mesh refining technique is employed close to the heated surface. The mesh has been established with node number $4.26 \cdot 10^6$ after mesh independent check.

Figure 3(a) shows the droplets spraying effect and the heat flux contours on the heated surface. Based on ANSYS Fluent post processing the overall sauter mean diameter (SMD) in the flow field is summarized to be 41.6 μm. Comparably, the droplet particles in physical experiment have an average diameter of 36.5 μm tested by a shadowgraph system [11]. For heat transfer performance the mean heat flux of a radial clip with diameter 12 mm is checked. Figure 3(b) shows the heat fluxes at different wall temperatures in simulations and experiments [11]. Same trend is shown as increasing wall temperature could improve the heat transfer performance. In a word, good agreements with a difference of 13% in SMD and error less than 20% in heat flux variation could be achieved which signifies that the numerical model is correct or reasonable at least. Hence the model could be applied for following simulations.

Results and discussion

Following the simulation procedures in model validation part, a 3-D domain outside the drum wall is established. Local mesh refining technique is employed to refine the mesh close to the drum wall. The mesh node number is $7.8 \cdot 10^6$ after mesh independence verification, fig. 2(b). It takes about 32 hours for simulating a flow time of 0.5 second on the Intel I7 processor with 8 cores. Only the heat transfer performance is focused in following

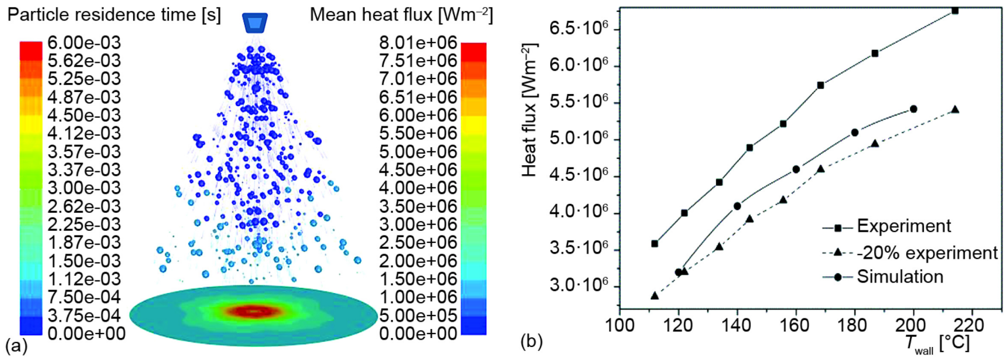

Figure 3. (a) The droplet spraying effect with heat flux contours on heated surface after convergence (t = 0.5 s, T_{wall} = 200 °C), (b) comparison of heat flux results under different wall temperature between simulation and experiment [11] (*for color image see journal web site*)

sections due to paper length limitations. Section *Analysis of spray cooling process* analyzes the spray cooling process of the basic case (P = 0.6 Mpa, T_{wall} =673 K, T_{water} = 282 K, spray height = 0.36 m). Parametric studies with single parameter changing are discussed in chapters on effects of upstream, spray height, water temperature, and wall temperature on heat flux, later in this paper. At last the influencing extents of studied parameters have been explored by Taguchi orthogonal experimental method.

Analysis of spray cooling process

When droplets interacted with the wall at the beginning, the local transient heat flux was greatly high to the order of 10^6 W/m^2 due to direct evaporation. However, the mean area-weighed heat flux on the whole curve wall was much smaller, about $5\cdot10^3$ W/m^2. As time went by, the number of droplets reaching the wall increased and then remained stable. The average wall heat flux also increased and gradually maintained a balance to about $4\cdot10^4$ W/m^2. Figure 4(a) shows the variation of average wall heat flux. It took about 0.13 second to reach relatively stable stage. The heat flux in the relatively stable stage would keep fluctuating, which was because the droplet distributions on the wall were different over time. Figure 4(b) shows a spray effect picture when t = 0.5 second.

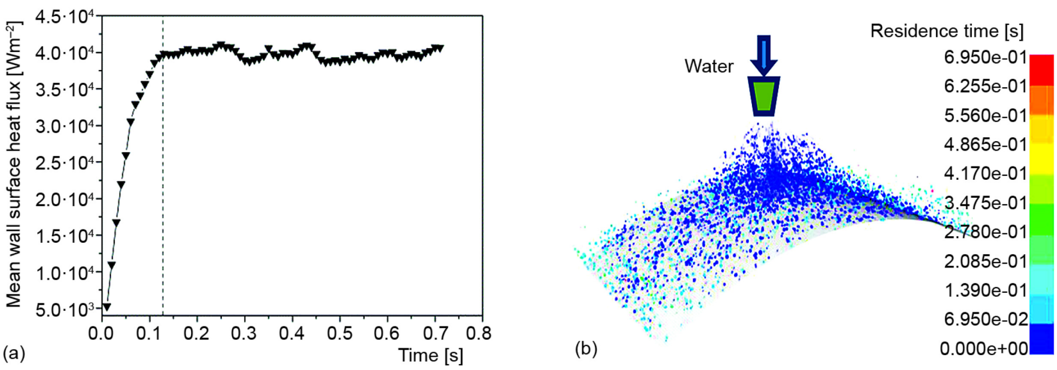

Figure 4. (a) Variation of area-weighed mean wall heat flux, (b) simulation diagram of single-nozzle spray (t = 0.5 s) (*for color image see journal web site*)

The heat transfer process remained steady after convergence, and fig. 5(a) shows the mean heat flux contours. The distribution shows concentric elliptical rings and the heat flux decreases with increasing elliptical radius. Lines A and B are the two axes of the elliptical rings. The two lines intersect at the center or stagnant point O, and the mean heat fluxes on both lines are shown in fig. 5(a). The minimum heat flux is about $2\cdot 10^4$ W/m^2 and the highest reaches the order of 10^5 W/m^2. It is worth noting that some experimental spray cooling could reach to 10^6 W/m^2 with strict conditions such as extremely small droplet diameters. These results coincide well with published findings [4]. It could be found in fig. 5(b) that no big differences exist in values of lines A and B which indicates that the effect of wall curvature is not remarkable yet because the wall diameter is much larger than the spray feature size namely spray height.

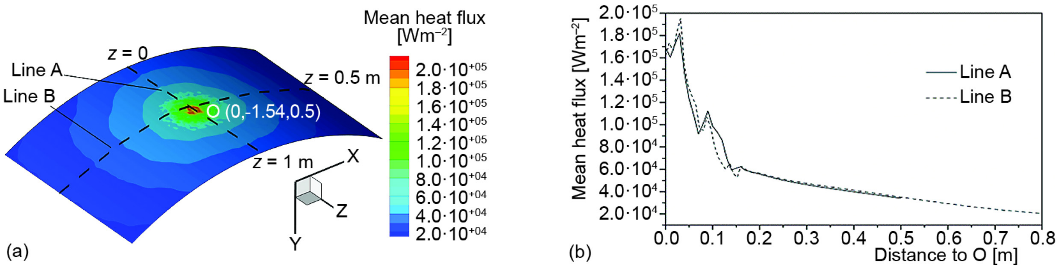

Figure 5. (a) Mean heat flux contours of simulated drum wall, (b) mean heat flux of different positions to stagnation point (*for color image see journal web site*)

Effect of upstream pressure on heat flux

For a certain nozzle if the upstream pressure changes, the mass-flow rate will correspond. The change follows the orifice flow law which is given by $Q_1/Q_2 = \sqrt{P_1}/\sqrt{P_2}$, where Q_1, Q_2, P_1, and P_2 correspond to different mass-flow rates and pressures. The flow path of the nozzle is 2.0 mm, and the design pressure and flow rate are 0.6 Mpa and 6.0 liter per minute, respectively. Four upstream pressures, *i. e.* 0.3, 0.4, 0.5, and 0.6 MPa (the flow rates are 0.0707, 0.0816, 0.0912, and 0.1 kg/s) have been simulated in this section. The top view of mean heat flux contours is given in fig. 6(a). The contours are displayed as concentric circle rings, rather than elliptical ones, due to change in view orientation. Figure 6(b) shows the change of area-weighed mean wall heat flux with upstream pressure. The heat flux enhances with increasing pressures and their relationship can be fitted as $\bar{q} = 29854 + 701.4\mathrm{e}^{4.4285p}$, where $\bar{q}$ [Mm^{-2}] is the mean heat flux and p [MPa] – the upstream pressure.

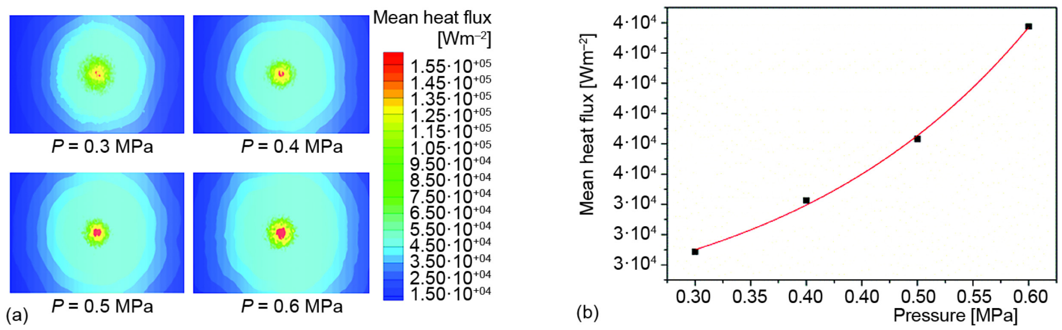

Figure 6. (a) Contours of mean heat flux under different upstream pressures, (b) relationship between area-weighed wall heat flux and the upstream pressure (*for color image see journal web site*)

Effect of spray height on heat flux

Spray height is an important design parameter. In this section the spray cooling performance for different spray heights at 270, 300, 330, and 360 mm, have been analyzed. Figures 7(a) and 7(b) show the corresponding top views of heat flux contours and the variations of mean heat fluxes with spray heights. It could be found that the mean heat flux keeps almost unchanged. However, descending heights will reduce spray area directly for the spray angle is fixed. Therefore, it can be inferred that the heat flux increases with decrease of spray height in effective spray areas.

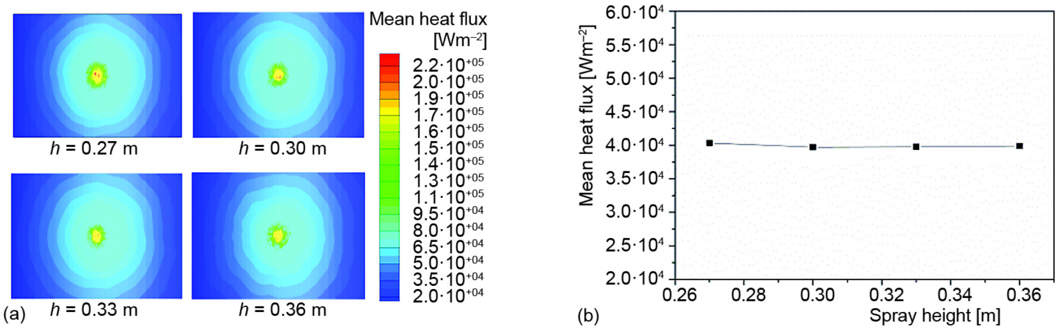

Figure 7. (a) Contours of mean heat flux under different spray heights, (b) variation of area-weighed mean wall heat flux with different spray heights (*for color image see journal web site*)

Effect of water temperature on heat flux

As is well-known, the temperature of cooling medium can directly affect heat transfer. In this section effects of different water temperatures at 282, 288, 293, and 298 K on spray cooling have been simulated. Figure 8(a) shows the mean heat flux contours. As expected the heat flux decreases gradually with increasing water temperature. The relationship among them shown in fig. 8(b) could be fitted as $\overline{q} = 3.61\cdot10^4 + 3.767\cdot10^{19}\cdot e^{-0.13t}$, where $\overline{q}$ [Wm^{-2}] is the mean wall heat flux and t [K] – the water temperature.

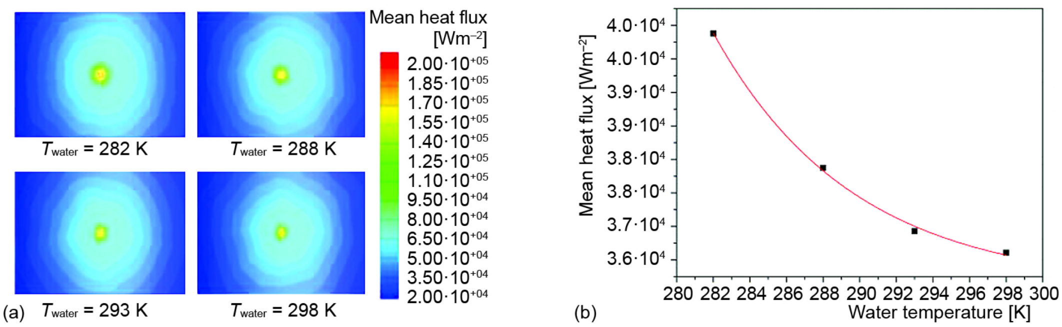

Figure 8. (a) Contours of mean heat flux under different water temperature, (b) relationship between area-weighed mean wall heat flux and water temperature (*for color image see journal web site*)

According to the Newton's law of cooling (given by $q = h\Delta t$, where h is the surface heat transfer coefficient), the heat flux has linear relationship with temperature difference if h

is constant. For example in a heat exchange tube without phase change the heat flux would change linearly with heat transferring medium temperature. In the simulated spray cooling, however, the change becomes non-linear. The heat fluxes increase with decreasing water temperatures which indicates that the surface heat transfer coefficient has altered following water temperature change. The reason mainly depends on phase change in the spray cooling processes.

Effect of wall temperature on heat flux

Spray cooling is always applied where heat source temperature is greater than vaporization temperature of cooling medium. The higher the heat source temperature is, the quicker the vaporization happens. Therefore, the wall temperature is of much significance to spray cooling process. Different wall temperatures at 373, 473, 573, and 673 K have been simulated in this section and the mean heat flux contours are shown in fig. 9(a). It can be seen that the heat flux is up to the order of 10^4 W/m^2 when the wall temperature is at 373 K, while up to the order of 10^5 W/m^2 when at 473, 573, and 673 K. As expected the mean wall heat flux increases with rising wall temperatures. Their relationship shown in fig. 9(b) can be fitted as $\overline{q} = 14053 \cdot e^{t/546} - 8445.5$, with R-squre 0.993, where $\overline{q}$ [Wm^{-2}] is the mean wall heat flux and t [K] – the wall temperature.

When the wall temperature is low, phase transition process is not dominated and convection is the main heat transfer mechanism. When the wall temperature is much higher than the cooling water saturation temperature (T = 373 K at 1 atm), the droplet vaporization process, that is to say, phase change is prominent, resulting in a considerable improvement of heat flux.

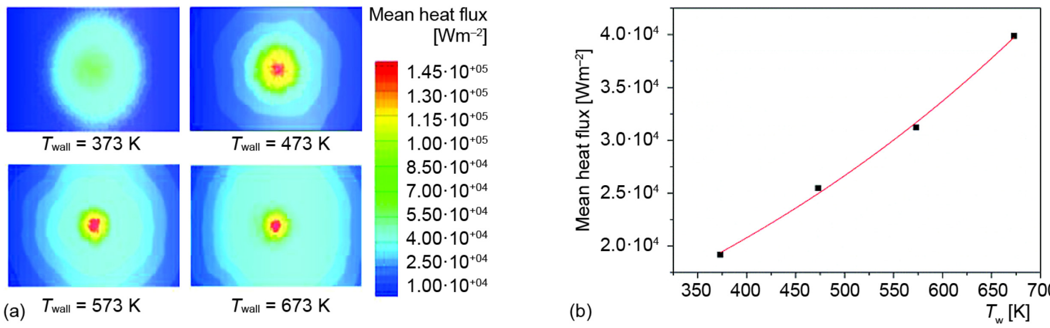

Figure 9. (a) Contours of mean heat flux under different wall temperatures, (b) relationship between area-weighed mean wall heat flux and wall temperature

Comparison of parameter influence degrees

In this section the Taguchi orthogonal experimental method has been employed to compare the influence degrees of the aforementioned four parameters on average wall heat flux. Each factor has four levels so the scale of the orthogonal experimental design is $L_{16}(4^4)$, where L is the symbol of orthogonal experimental, 16 – the number of experiments, "4" – the 4 levels, and its superscript "4" – the 4 factors. An orthogonal experimental list with 16 cases is shown in tab. 2. All the results have been obtained with corresponding conditions (see tab. 2) by following the same computing methods.

It can be found that the influencing degrees of the four factors on the mean wall heat flux are: wall temperature > pressure > water temperature > spray height (by comparing F

Table 2. The $L_{16}(4^4)$ orthogonal experimental list and results

Case number	T_{wall}, [K]	Pressure, [MPa]	T_{water}, [K]	Height, [m]	Mean heat flux, [Wm^{-2}]
1	473	0.5	282	0.27	24761.22
2	373	0.4	282	0.33	17921.4
3	573	0.3	282	0.3	25466.38
4	673	0.5	298	0.33	34398.18
5	373	0.5	293	0.3	18223.87
6	573	0.6	293	0.33	29476.96
7	673	0.3	293	0.27	31991.17
8	573	0.5	288	0.36	27042.19
9	673	0.6	282	0.36	38237.6
10	673	0.4	288	0.3	32155.79
11	473	0.4	293	0.36	17995.85
12	573	0.4	298	0.27	25510.54
13	473	0.6	298	0.3	21765.68
14	473	0.3	288	0.33	18398.02
15	373	0.6	288	0.27	20457.15
16	373	0.3	298	0.36	14679.75

values). The effects of wall temperature, pressure and water temperature show significant (Sig. < 0.05) while the effect of spray height is not outstanding. The results could give many instructions to industry practice. For example the former three arguments should be focused, controlled strictly and maintained well for their importance. While for the spray height, a larger value could be selected when designing a spray cooling system, which on one hand is beneficial to installation and maintenance of spray devices and on the other hand will not affect heat transfer performance to a great extent.

Variance analysis has been implemented to the orthogonal test results in tab. 2 and the analysis summary is followed in tab. 3.

Table 3. Variance analysis of the orthogonal experimental design

Variance source	Sum of squares of mean deviation	d_f	Mean square	F	Sig.
Wall temperature	6.31E+08	3	2.10E+08	487.32	0.000
Upstream pressure	6.21E+07	3	2.07E+07	47.962	0.005
Water temperature	1.57E+07	3	5.22E+06	12.09	0.035
Spray height	4.19E+06	3	1.40E+06	3.232	0.181
Error	1.30E+06	3	4.32E+05		

Conclusions

In this work the large scale industry applied spray cooling on curve wall has been simulated with verified numerical model. Effects of upstream pressure, spray height, water temperature, and wall temperature on the mean wall heat flux have been studied for a certain industrial solid-cone pressure swirl nozzle. It is found that the mean heat flux distributions are concentric elliptical rings on the curve wall. The mean heat flux increases with increasing upstream pressures and an exponential law could be fitted between them. The area-weighed heat flux on the whole curve wall keeps almost unchanged with decreasing spray heights, which infers to that the mean heat flux in the direct spray area on the curve wall enhances with descending heights. The water temperature and wall temperature determine superheat together and they are of much significance. Decreasing water temperature or increasing wall temperature will strengthen the heat flux and *vice versa*. Both cases show exponential relationship.

The influencing degrees of the four studied variables have also been compared by the Taguchi orthogonal experimental method and the result is: wall temperature > pressure > water temperature > spray height. The effects of wall temperature, pressure and water temperature are significant while the effect of spray height is not.

Acknowledgments

The China Scholarship Council (No. 201406950059) and the Enterprise cooperative Project of Wuhan University of Technology (No. WHUT-20162h0149) are gratefully thanked for financial support of this work.

Nomenclature

A_p – surface of droplet, [m^2]
C_D – drag coefficient, [–]
c_p – specific heat, [Jkg^{-1}K^{-1}]
d_p – particle diameter, [m]
E – heat energy, [J]
F – force on particle in control volume, [kgms^{-2}]
g – gravity acceleration, [ms^{-1}]
h_{fg} – latent heat, [Jkg^{-1}]
h_{pyrol} – heat of pyrolysis, [Jkg^{-1}]
k – thermal conductivity, [Wm^{-1}K^{-1}]
M – the particle mass change in control volume, [kgs^{-1}]
$m_{p,0}$ – the initial mass of particle, [kg]
Δm_p – mass change of a particle as it passes through each control volume, [kg]
$\dot{m}_p$ – mass-flow rate of particles, [kgs^{-1}]
$\dot{m}_{p,0}$ – the initial particle mass-flow rate, [kgs^{-1}]
Pr – Prandtl number of continuous phase, [–]
p – pressure, [Nm^{-2}]
Re – relative Reynolds number, [–]
S – source term [–]
T – temperature, [K]
Δt – time step, [s]
$\vec{U}$ – fluid velocity vector, [ms^{-1}]
u – fluid velocity, [ms^{-1}]

Greek symbols

ε – emissivity, [–]
η – dynamic viscosity, [Pa·s]
μ – molecular viscosity of the fluid, [kgm^{-1}s^{-1}]
ρ – density, [kgm^{-3}]
σ – Stephen Boltzmann constant, [Wm^{-2}K^{-4}]

Subscripts

f – continuous fluid phase
p – particles /droplets

References

[1] Horacek, B., *et al.*, Single Nozzle Spray Cooling Heat Transfer Mechanisms, *International Journal of Heat and Mass Transfer*, *48* (2005), 8, pp. 1425-1438
[2] Cader, T., *et al.*, Spray Cooling Thermal Management for Increased Device Reliability, *IEEE Transactions on Device & Materials Reliability*, *4* (2005), 4, pp. 605-613
[3] Basinger, B., *et al.*, Effect of Skin Indentation on Heat Transfer during Cryogen Spray Cooling, *Lasers in Surgery & Medicine*, *34* (2004), 2, pp. 155-163

[4] Mascarenhas, N., Mudawar, I., Analytical and Computational Methodology for Modeling Spray Quenching of Solid Alloy Cylinders, *International Journal of Heat and Mass Transfer*, *53* (2010), 25-26, pp. 5871-5883
[5] Ebrahimian, V., Gorji-Bandpy, M., Two-Dimensional Modeling of Water Spray Cooling in Superheated Steam, *Thermal Science*, *12* (2008), 2, pp. 79-88
[6] Liang, G., Mudawar, I., Review of Spray Cooling – Part 1: Single-Phase and Nucleate Boiling Regimes, and Critical Heat Flux, *International Journal of Heat & Mass Transfer*, *115* (2017), Part A, pp. 1174-1205
[7] Liang, G., Mudawar, I., Review of Spray Cooling – Part 2: High Temperature Boiling Regimes and Quenching Applications, *International Journal of Heat & Mass Transfer*, *115* (2017), Part A, pp. 1206-1222
[8] Lee, D., Irmawati, N., Investigation on Fluid Flow and Heat Transfer Characteristics in Spray Cooling Systems Using Nanofluids, *Dynamics*, *9* (2015), 8, pp. 1409-1413
[9] Wen, D., *et al.*, Review of Nanofluids for Heat Transfer Applications, *Particuology*, *7* (2009), 2, pp. 141-150
[10] Cheng, W., *et al.*, An Experimental Investigation of Heat Transfer Enhancement by Addition of High-Alcohol Surfactant (HAS) and Dissolving Salt Additive (DSA) in Spray Cooling, *Experimental Thermal and Fluid Science*, *45* (2013), Feb., pp. 198-202
[11] Zhang, Z., *et al.*, Experimental Investigation of Spray Cooling on Flat and Enhanced Surfaces, *Applied Thermal Engineering*, *51* (2013), 1-2, pp. 102-111
[12] Xie, J. L., *et al.*, Study of Heat Transfer Enhancement for Structured Surfaces in Spray Cooling, *Applied Thermal Engineering*, *59* (2013), 1-2, pp. 464-472
[13] Silk, E. A., *et al.*, Spray Cooling of Enhanced Surfaces: Impact of Structured Surface Geometry and Spray Axis Inclination, *International Journal of Heat and Mass Transfer*, *49* (2006), 25, pp. 4910-4920
[14] Sodtke, C., Stephan, P., Spray Cooling on Micro Structured Surfaces, *International Journal of Heat and Mass Transfer*, *50* (2007), 19-20, pp. 4089-4097
[15] Jia, W., Qiu, H. H., Experimental Investigation of Droplet Dynamics and Heat Transfer in Spray Cooling, *Experimental Thermal and Fluid Science*, *27* (2003), 7, pp. 829-838
[16] Liu, X., *et al.*, Flow Characteristics of Liquid Nitrogen through Solid-Cone Pressure Swirl Nozzles, *Applied Thermal Engineering*, *110* (2017), Suppl. C, pp. 290-297
[17] Vouros, A., *et al.*, Experimental Study of a Water-Mist Jet Issuing Normal to a Heated Flat Plate, *Thermal Science*, *20* (2016), 2, pp. 149-149
[18] Ichikawa, H., Morishige, H., Rotary Hearth Furnace Process for Steel Mill Waste Recycling and Direct Reduced Iron Making, *Revue De Metallurgie*, *100* (2003), 4, pp. 349-354
[19] *** Inc, A., ANSYS Fluent Theory Guide, http://www.ansys.com

Paper submitted: September 20, 2017
Paper revised: November 15, 2017
Paper accepted: November 17, 2017